

Colloidal Nanoplatelets-Based Soft Matter Technology for Photonic Interconnected Networks: Low-Threshold Lasing and Polygonal Self-Coupling Microlasers

Rui Duan,* Yi Tian Thung, Zitong Zhang, Emek Goksu Durmusoglu, Yichen He, Lian Xiao, Calvin Xiu Xian Lee, Wen Siang Lew, Lin Zhang, Hanyang Li, Jun Yang, Hilmi Volkan Demir,* and Handong Sun*

Soft matter-based microlasers are widely regarded as excellent building blocks for realizing photonic interconnected networks in optoelectronic chips, owing to their flexibility and functional network topology. However, the potential of these devices is hindered by challenges such as poor lasing stability, high lasing threshold, and gaps in knowledge regarding cavity interconnection characteristics. In this study, the first demonstration of a high-quality, low-threshold nanoplatelets (NPLs)-based polymer microfiber laser fabricated using capillary immersion techniques and its photonic interconnected networks are presented. CdSe/CdS@Cd_{1-x}Zn_xS core/buffer shell@graded-shell NPLs with high optical gain characteristics are adopted as the gain medium. The study achieves a lasing threshold below 14.8 $\mu\text{J cm}^{-2}$, a single-mode quality (Q)-factor of ≈ 5500 , and robust lasing stability in the fabricated NPLs-based microfibers. Furthermore, the study pioneers the exploration of polygonal self-coupling microlasers and the optical characteristics of their interconnected fiber network. Based on the signal generation mechanism observed in the photonic networks, an interconnected NPLs-based fiber network structure achieving single-mode lasing emission and laser mode modulation is successfully designed. The work contributes a novel method for realizing microlasers fabricated via soft-matter technologies and provides a key foundation and new insights for unit design and programming for future photonic network systems.

1. Introduction

Micro- and nanolasers are critical in the development and refining of areas such as low threshold laser sources,^[1-5] highly sensitive sensors,^[6-10] optical neural network stimulatory components,^[11,12] and multiplexers applicable to mathematical logic.^[13-16] These coherent light sources provide extremely high spectral purity and directionality, and micron- or nanometer-sized active devices are essential for enhancing the integrational capability per unit volume and resulting computing power befitting. Soft matter microfibers and 1D nanowires exhibit superb optical properties, including high flexibility, ease of doping, and functional network topology,^[17-22] making them ideal building blocks for efficient coherent light sources and nanophotonic networks. Previous demonstrations attested how polymer fibers can be conveniently fabricated via electrospinning^[18,23-25] or direct drawing,^[21,26-29] allowing for assembly and manipulation of arbitrary structures in soft matter

R. Duan, Y. T. Thung, Z. Zhang, E. G. Durmusoglu, L. Xiao, C. X. X. Lee, W. S. Lew, H. V. Demir, H. Sun
Division of Physics and Applied Physics
School of Physical and Mathematical Sciences
Nanyang Technological University
21 Nanyang Link, Singapore 637371, Singapore
E-mail: rui.duan@ntu.edu.sg; hvdemir@ntu.edu.sg; hdsun@ntu.edu.sg
Y. T. Thung, E. G. Durmusoglu, H. V. Demir
LUMINOUS! Centre of Excellence for Semiconductor Lighting and Displays
The Photonics Institute
School of Electrical and Electronic Engineering
Nanyang Technological University
Singapore 639798, Singapore

Z. Zhang
Xi'an Modern Chemistry Research Institute
Xi'an, Shaanxi 710065, China
Y. He, L. Zhang
School of Precision Instruments and Optoelectronics Engineering
Tianjin University
Tianjin 300072, China
H. Li
College of Physics and Optoelectronic Engineering
Harbin Engineering University
Harbin 150001, China
J. Yang
Guangdong Provincial Key Laboratory of Information Photonics
Technology
College of Information Engineering
Guangdong University of Technology
Guangzhou 510006, China

 The ORCID identification number(s) for the author(s) of this article can be found under <https://doi.org/10.1002/lpor.202300745>

DOI: 10.1002/lpor.202300745

micron- and nanolasers to make targeted interactions with various components in a photonic system. The resulting polymer fiber system is one of the best building blocks for actualizing highly interconnected complex photonic networks.^[17–19] However, most soft matter microlasers still adopt traditional organic dyes as their gain medium, rendering concerns about photochemical stability and fluorescence quenching, which are the biggest obstacles to their practical applications.

The potential and advantages of miniaturized laser light sources are yet to be fully realized, despite previous reports heralding the unparalleled developmental opportunities that optoelectronic applications employing colloidal nanoplatelets (NPLs) with 1D quantum confinement^[30–32] as the active medium^[33–37] can provide. These NPLs offer superior optoelectronic properties compared to their 0D and traditional organic dye counterparts, including high chemical stability,^[3,38,39] narrow emission linewidth,^[40,41] large absorption cross-section,^[42–44] and suppressed nonradiative Auger recombination,^[45–47] which have generated considerable interest. However, despite the NPLs' integral role in fabricating micro- and nanolasers, current efforts are only limited to detailed studies of solid NPLs lasers.^[3,48–53] Representative past works include demonstrating the waveguide properties and high modal gain coefficient of NPLs via using a coreless fiber as a host cavity,^[38] and the integration of NPLs and silica microspheres to provide an ultralow threshold of 3.26 $\mu\text{J cm}^{-2}$ at room temperature.^[3] In our recent work, we have realized a high lasing Q -factor of 13000 from a double-layered NPLs gain film using the self-assembly of NPLs driven by liquid interface dynamics.^[48] The low mechanical flexibility of solid lasers manifests as irreparable disadvantages. To fully realize the potential of NPLs as a lasing gain medium for a wider range of applications, alternative forms of resonant cavities must be implemented. Specifically, there has been no previous report on lasing studies of colloidal NPLs integrated with soft matter to date, which can overcome the disadvantages of solid NPLs lasers.

In this work, we introduce a new type of capillary immersed NPLs-based polymer microfiber lasers that demonstrate high-quality, low-threshold lasing performance. Our approach utilizes CdSe/CdS@Cd_{1-x}Zn_xS core/buffer shell@graded-shell NPLs with high optical gain as the lasing medium, marking the first successful implementation of colloidal semiconductor NPLs in soft matter lasing devices. Through careful size control, we achieve multimode and single-mode lasing of high quality (Q -) factor and robust lasing stability, far surpassing traditional organic dye-doped fiber lasers. We provide a comprehensive analysis of the optical characteristics and lasing types of microfiber lasers fabricated via surface coating of colloidal NPLs. Leveraging the outstanding optical gain characteristics of colloidal NPLs

and the mechanical flexibility of soft matter microfiber cavities, we pioneer a study on polygonal self-coupling NPLs microfiber lasers and their interconnected fiber network system. Additionally, the high-quality single-mode lasing has been realized from the as-designed interconnected fiber network system. Our work documents a new application of NPLs as a gain medium, and a new format of soft-matter technology-directed lasers. By combining these new concepts and technologies together, this work provides a key foundation and new insights for unit design and programming for future photonic network systems.

2. Results and Discussion

2.1. Characterization of CdSe/CdS@Cd_{1-x}Zn_xS NPLs and NPLs-Based Microfibers

We synthesized red-emitting CdSe/CdS@Cd_{1-x}Zn_xS core/alloyed-shell NPLs by following the procedures proposed by Kelestemur et al.^[36] with slight modifications for optimization. These NPLs have a hybrid-shell structure that we engineered specifically, resulting in excellent optical gain characteristics and a low excitation threshold. Therefore, we selected them as the gain medium for our desired soft matter microfiber lasers. The as-synthesized NPLs are highly monodisperse and size-uniform, displaying a photoluminescence (PL) of 656.8 nm with a full-width half-maximum (FWHM) of ≈ 21 nm when dispersed in hexane (Figure 1a), with a high photoluminescence quantum yield (PLQY) of 96 %. The bright-field transmission electron microscopy (TEM) in Figure 1b and Figure S1 (Supporting Information) shows that the NPLs have a uniform quadrilateral shape. We evaluated their excellent gain properties via amplified spontaneous emission (ASE) using a variable stripe excitation geometry under femtosecond laser pumping (Figure S2, Supporting Information). Figure 1c displays a narrower emission band on the red side of the spontaneous emission band emerging with increasing femtosecond pump fluence. This indicates the appearance of stimulated emission and affirms the multi-excitonic gain mechanism in the NPLs. The inset shows that the integrated pump intensity depends on pump fluence to indicate a low ASE threshold of $\approx 4.4 \mu\text{J cm}^{-2}$, highlighting the suitability of these NPLs to be employed as the gain medium for our desired soft matter microfiber lasers.

A microcavity lasing device is distinguished by its smooth cavity surface and excellent cavity gain. These two critical factors are achieved by strategically positioning NPLs-based soft matter polymer fibers. By leveraging capillary immersive forces, NPLs are carefully deposited onto the fibers, resulting in a tightly packed and smooth coating (Figure 1d,e). The energy dispersive spectroscopy (EDS), as shown in Figure 1f–i, affirms this preparation method's outstanding quality and practical feasibility through its highly uniform and dense elemental distribution. Additionally, surface profiling studies via atomic force microscopy (AFM) indicate the thickness of the NPLs gain layer is ≈ 117 nm (Figure S3, Supporting Information). Another interesting insight is derived from the 1D nanowire-like structures of polymer fiber based on NPLs. The significant difference in refractive indices between 1D resonant cavities and their surrounding environment makes them suitable for use as an excellent nanoscale light source. Furthermore, the mechanical flexibility and ease of manipulation of

H. V. Demir
School of Materials Science and Engineering
Nanyang Technological University
Singapore 639798, Singapore

H. V. Demir
Department of Electrical and Electronics Engineering
Department of Physics
UNAM—Institute of Materials Science and Nanotechnology
Bilkent University
Ankara 06800, Turkey

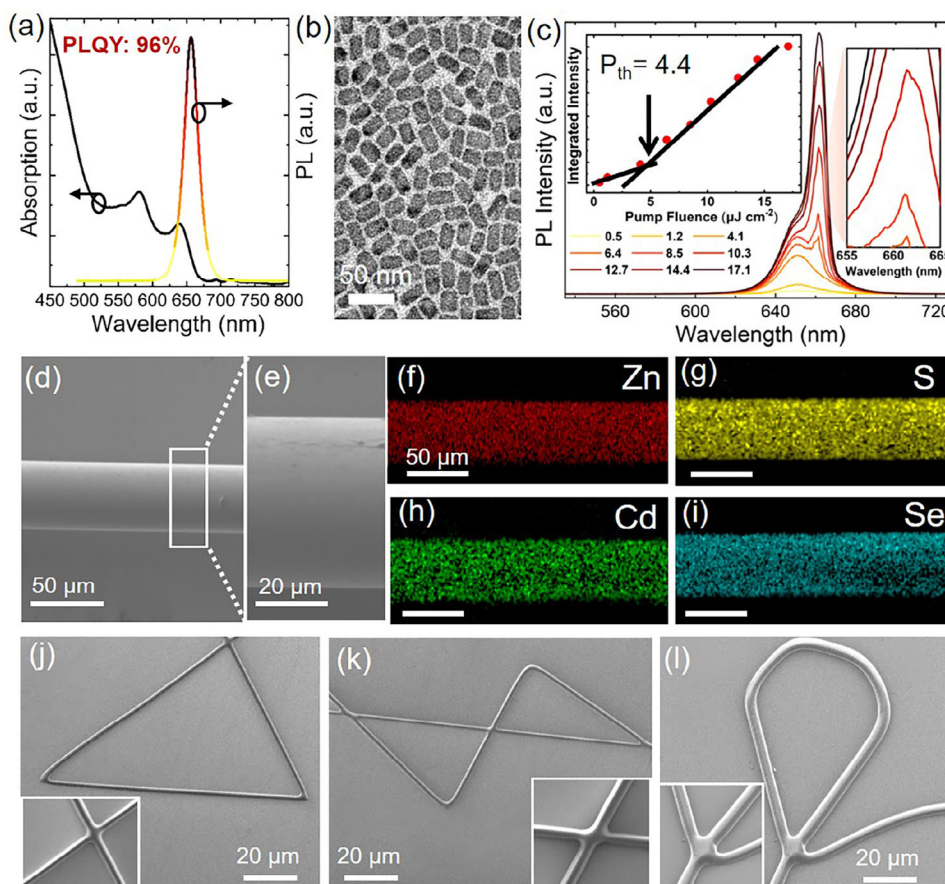


Figure 1. a) Absorbance and photoluminescence spectra of the CdSe/CdS@Cd_{1-x}Zn_xS core/buffer shell@graded-shell NPLs and its PLQY at room temperature. b) Annular bright-field TEM images of 4ML as-synthesized NPLs. c) ASE spectra of as-synthesized core/shell NPLs under femtosecond pumping with different pump fluence. Inset: The integrated edge emission intensity with the pump intensity. d) SEM image of NPLs-coated polymer microfiber. e) A zoomed-in image shows more detail about the surface. f–i) EDS mapping of NPLs-coated polymer microfiber reveals the uniform and dense distribution of Zn, S, Cd, and Se elements on the microfiber surface. j–l) SEM images of NPLs-self-coupled cavity with triangular, double interconnection triangular, and pentagonal configurations.

polymer materials allow for the easy creation of a wide array of microcavities with assorted shape configurations (Figure 1j–l). Moreover, the high viscosity and superb cohesiveness of epoxy resin in the polymer mixture enable two discrete nanowires to demonstrate perfect fusion when intersecting (Figures S4 and S5, Supporting Information). This configuration facilitates the formation of a truly closed loop for the self-coupling resonator, as opposed to evanescent wave coupling typical of traditional adaptations.

2.2. NPLs-Based WGM Lasing Microfiber

We characterized the NPLs-based soft matter microfiber lasers optically via a home-built micro-photoluminescence (μ -PL) system under ambient conditions (Figure 2a). Attributed to a smooth and denser gain layer, NPLs-based microfiber demonstrates a low lasing threshold and high lasing Q -factor. Figure 2b depicts the emission spectra of a 23 μ m-diameter NPLs-microfiber at various pump intensities, revealing sharp multimode lasing with FWHM \approx 0.11 nm. The non-linear increase of the rapidly boosted emis-

sion intensity with pump fluence confirms the onset of lasing action. Additionally, power-dependent PL measurements from these NPLs-based microfibers indicate a lasing threshold as low as \approx 14.8 μ J cm⁻², which is lower than the threshold values from previously reported microfiber lasers.^[27–29] To further validate the lasing behavior, we investigated the PL dynamics of the NPLs-coated polymer microfiber lasers below and above the threshold (Figure S6, Supporting Information). At a pump intensity significantly below the threshold, the PL decay follows a trajectory akin to spontaneous emission. Upon exceeding the threshold with a pump intensity, a rapid decay channel manifests, and the abrupt collapse of PL decay substantiates the onset of lasing action. The analysis of the PL decay curves before and after the threshold was added to Table S1 (Supporting Information). Nevertheless, in the forthcoming work, we will explore the utilization of kinetically driven liquid–liquid interface self-assembly methods for precise nanocrystal deposition,^[48,54] aiming to further enhance the surface smoothness of the cavity and consequently achieve a further reduction in the lasing threshold. The bright red emission observed from the edges of the microlaser in the inset of Figure 2b provides direct preliminary evidence that the lasing is of WGM

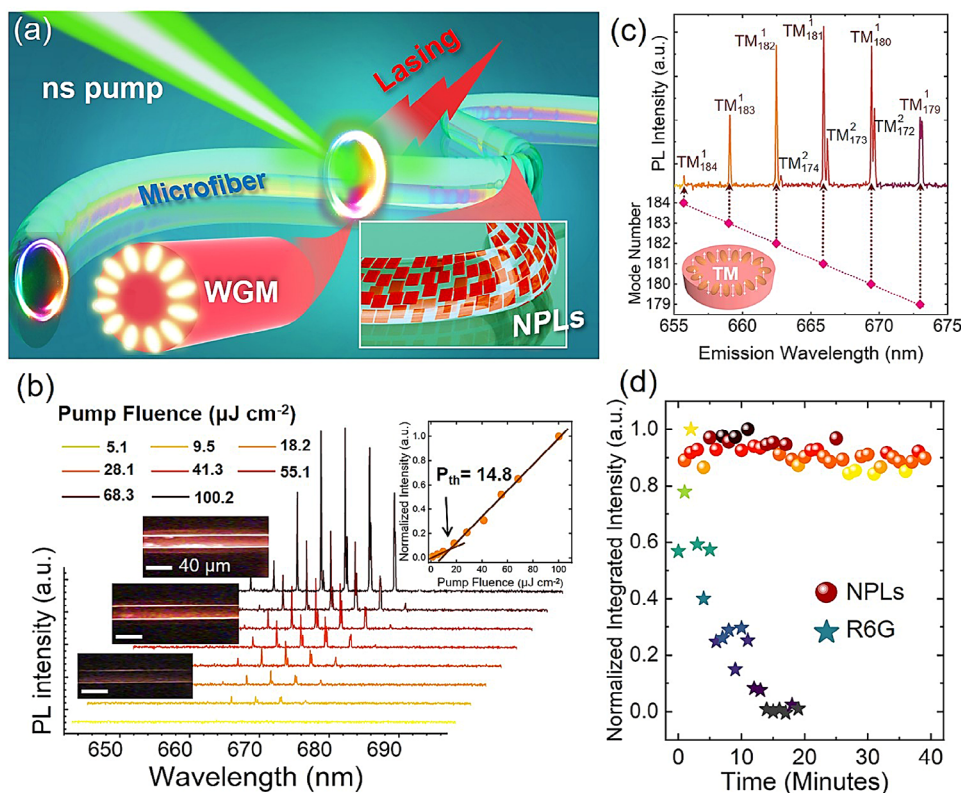


Figure 2. a) Schematic diagram of NPLs-coated polymer microfiber lasers in which the CdSe/CdS@Cd_{1-x}Zn_xS core/shell NPLs are uniformly covered on the surface of the polymer microfibers. b) Measured lasing spectra of NPLs-coated polymer microfiber at various pumping energy densities. The bright emission at the edge of the microlaser can be observed. The lasing threshold is determined to be $\approx 14.8 \mu\text{J cm}^{-2}$. c) Lasing mode analysis based on the WGM model. The lasing peaks fit well with the fundamental and second-order TM modes. d) The normalized lasing intensity of NPLs- and R6G-based microfiber lasers under continuous pumping excitation (≈ 10 times lasing threshold). Distinct lasing intensities were discerned through the use of gradient colors.

type. Further theoretical analysis of the lasing modes affirms the WGM lasing mechanism of the NPLs-based microfiber, with the first and second order of the transverse magnetic (TM) mode identified from the lasing peaks (see Figure 2c and Experimental and Simulation Section S9, Supporting Information). The regression equation of the fitting curves between mode numbers and excitation wavelength, along with the coefficient of determination (represented by R^2), has been provided in Figure S7 (Supporting Information).

The photostability of soft matter microfiber lasers is the most critical bottleneck restricting their practical applications. Traditional organic dyes often suffer from photobleaching and photodegradation, which limits their potential and use in laser networks and optical engineering. To demonstrate the superiority of NPLs-based soft matter polymer microfiber against their traditional organic dye (Rhodamine 6G)-doped counterpart, we studied the evolution of lasing intensities of two microfibers of different gain medium when excited under continuous and intense nanosecond laser pulse excitation (532 ns , $\approx 10 P_{th}$) at room temperature and ambient conditions. As depicted in Figure 2d, the lasing intensity of the organic dye-based microlaser decreases rapidly within 15 min of continuous laser pulse excitation. In stark contrast, no significant lasing intensity attenuation (less than 4 % decrease of intensity) is observed from the NPLs-based

microfiber over a monitoring period of up to 40 min when optically pumped. Such robust and stellar lasing stability establishes a good foundation for soft matter lasers in future practical engineering applications.

Upon closer observation, we found that the free spectral ranges (FSRs) of lasing peaks produced by the NPLs-based microfiber lasers decrease with increasing microfiber diameter, thereby demonstrating a clear inverse proportional relationship to further confirm the WGM nature (see Figure 3a,b; Figure S8, Supporting Information). The fluorescent images of NPLs-coated microfiber lasers with different diameters are presented in Figure S9 (Supporting Information). Furthermore, the microfibers with different diameters ranging from 10 to 60 μm (in increments of $\approx 10 \mu\text{m}$) we fabricated further demonstrate our controllability of fiber size (Figure S10, Supporting Information). By further reducing the diameter of the resonant cavity, we were able to achieve high-quality single-mode lasing. As shown in Figure 3c, we observed single-mode lasing emission at $\approx 656.25 \text{ nm}$, with an FWHM of $\approx 0.12 \text{ nm}$. Benefiting from the high optical gain of NPLs and smooth microfiber surface, the single mode lasing threshold is at a mere $\approx 24.4 \mu\text{J cm}^{-2}$ (Figure S11, Supporting Information). When the trade-off between cavity gain and losses was weighed, the lasing Q -factor showed an increasing trend with microfiber diameter before decreasing after an optimal diameter,

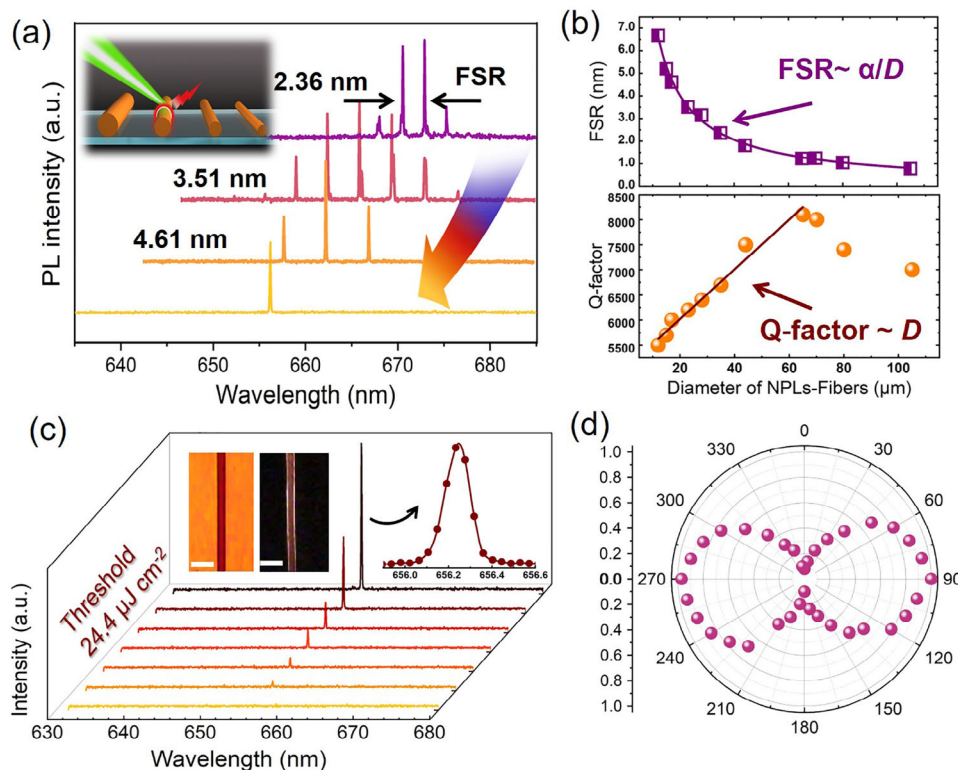


Figure 3. a) Lasing spectra of ≈ 35 , ≈ 23 , ≈ 17 , and ≈ 7 μm NPLs-coated microfiber lasers. The FSRs corresponding to the first three sizes are 2.36, 3.51, and 4.61 nm, respectively. b) Upper panel: the inverse proportional fitting curve of the cavity size and the FSR, which further confirms the WGM mechanism; Lower panel: the dependence function of lasing Q -factor on cavity size. The Q -factor showed a trend of increasing first and then decreasing with the diameter. c) Single frequency emission of NPLs-coated polymer microfiber with a diameter of ≈ 7 μm . The lasing threshold was measured at ≈ 24.4 $\mu\text{J cm}^{-2}$ and the linewidth was ≈ 0.12 nm. Scale bar: 20 μm . d) Dependence of lasing mode intensity as the rotation angle of the polarizer.

consistent with the conclusions from our previous work (lower panel of Figure 3b).^[3] The notable performance of NPLs-based soft matter microfiber lasers can be attributed to three unique advantages: i) NPLs with excellent gain and high PLQY are used as gain media. ii) Compact and smooth film formation obtained by NPLs coating through capillary immersive forces significantly reduces scattering losses at the interface. iii) The WGMs provide strong optical confinement for laser oscillation in NPLs-coated microfibers. As shown in Figures S12 and S13 (Supporting Information), the circulating light is effectively confined within the microcavity through total internal reflection, with only 4.6% and 1.4% of the energy leaking out in the form of evanescent waves into the surrounding air and the unexcited axial domain of the microfiber.

We also investigated the polarization anisotropy of the NPLs-based microfiber laser by comparing the dependence of lasing mode intensity as a function of polarizer rotation angle under constant excitation intensity, as depicted in Figure 3d. The polarization factor was determined to be 0.925, indicating the excellent polarization performance of the NPLs-based microfiber lasers and their capability to emit linearly polarized light (see Experimental and Simulation Section S10, Supporting Information for details). Furthermore, the mechanical tunability of the proposed soft-matter microfiber laser has also been confirmed. As shown in Figure S14 (Supporting Information), due to the flexibility of the NPLs-coated microfibers, we achieved highly

sensitive tuning of the lasing wavelength by bending the fibers. This outcome offers a significant potential solution for wavelength modulation and packaging in NPLs-coated microfiber lasers.

2.3. NPLs-Based Self-Coupled Microlasers

Nanophotonic networks pave the way for a new architecture of laser devices, with the interaction between network basic units being the focus of research. In fact, the frequency at which polygonal cavities appear as the fundamental units in the photonic network is much higher than that of arc-shaped or circular cavities.^[17–19] Here, we present the interesting observation of soft microfibers with closed loops forming self-coupled resonators (Figure 4a). The submicron confinement along the diameter scale of the cavity forces light to oscillate in a self-coupling optical path, resulting in self-coupling resonance when the optical path of the resonator is equivalent to an integer multiple of the resonant wavelength. Although previous reports have demonstrated self-coupling lasing phenomenon from organic dye-based nanowires,^[18,21] these demonstrations have been limited to circular and arc-shaped structures. Therefore, there is a pressing need to understand the lasing performance of patterned microresonators of various geometries, and the viability of generating lasing action from such microresonators.

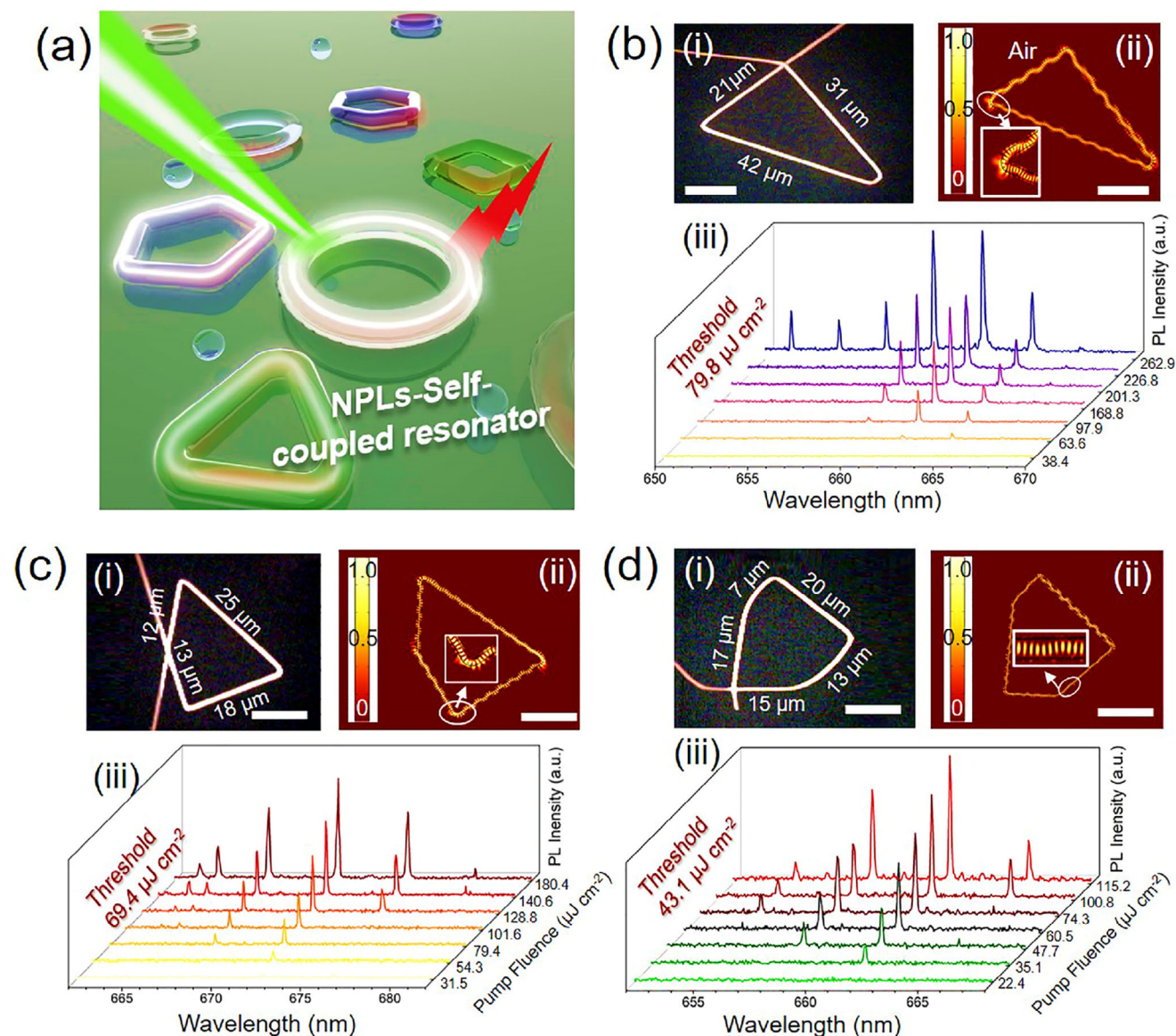


Figure 4. a) Schematic diagram of self-coupled NPLs-coated polymer microfiber lasers with different geometric shapes. b) (i) Dark-field PL microscope image of 1-D triangle-shaped self-coupled resonator. (ii) Numerical simulation of electric field for resonator (i). The magnified view reveals the transmission and scattering of the electric field at the corner of the cavity. (iii) Dependence of the lasing intensity on the pump fluence. c) (i) Dark-field PL image of the quadrilateral-shaped self-coupled resonator. (ii) Corresponding numerical simulation. (iii) Dependence of the lasing intensity on the pump fluence. d) (i) Dark-field PL image of the pentagon-shaped self-coupled resonator. (ii) Corresponding numerical simulation. The magnified view shows the transmission and resonance states of the light in the straight waveguide. (iii) Dependence of the lasing intensity on the pump fluence. Scale bars: 10 μm .

To address this research gap, we fabricated various polygonal microcavities encompassing triangular, quadrilateral, and pentagonal configurations. We leverage capillary immersive forces to assemble NPLs onto the surfaces of self-coupling cavities, forming a conformal coating on the cavities' surfaces and retaining their perfect polygonal configuration. The high viscosity and cohesiveness of epoxy resin allowed us to fuse two discrete nanowires perfectly at their intersection. The true closed loop demonstrated by these self-coupling resonators can significantly reduce circulation loss of resonant light as compared to their traditional evanescent coupling counterparts.

We experimentally demonstrated good manipulation of the spot size of the pump fluence, ensuring complete coverage of the resonant cavity. Bright fluorescent images revealed well-defined closed-loop polygonal configurations. Figure 4b–d demonstrate the generation of multimode lasing, indicated by the comb-like periodic lasing peak with increasing pump intensity, in fabricated polygonal microcavities with various configurations. The lasing thresholds, which provided direct evidence of the lasing action, were also determined by us. Interestingly, we observed a gradual reduction in the lasing threshold with the increment of the polygonal order of these microcavities. As shown in Figure S15

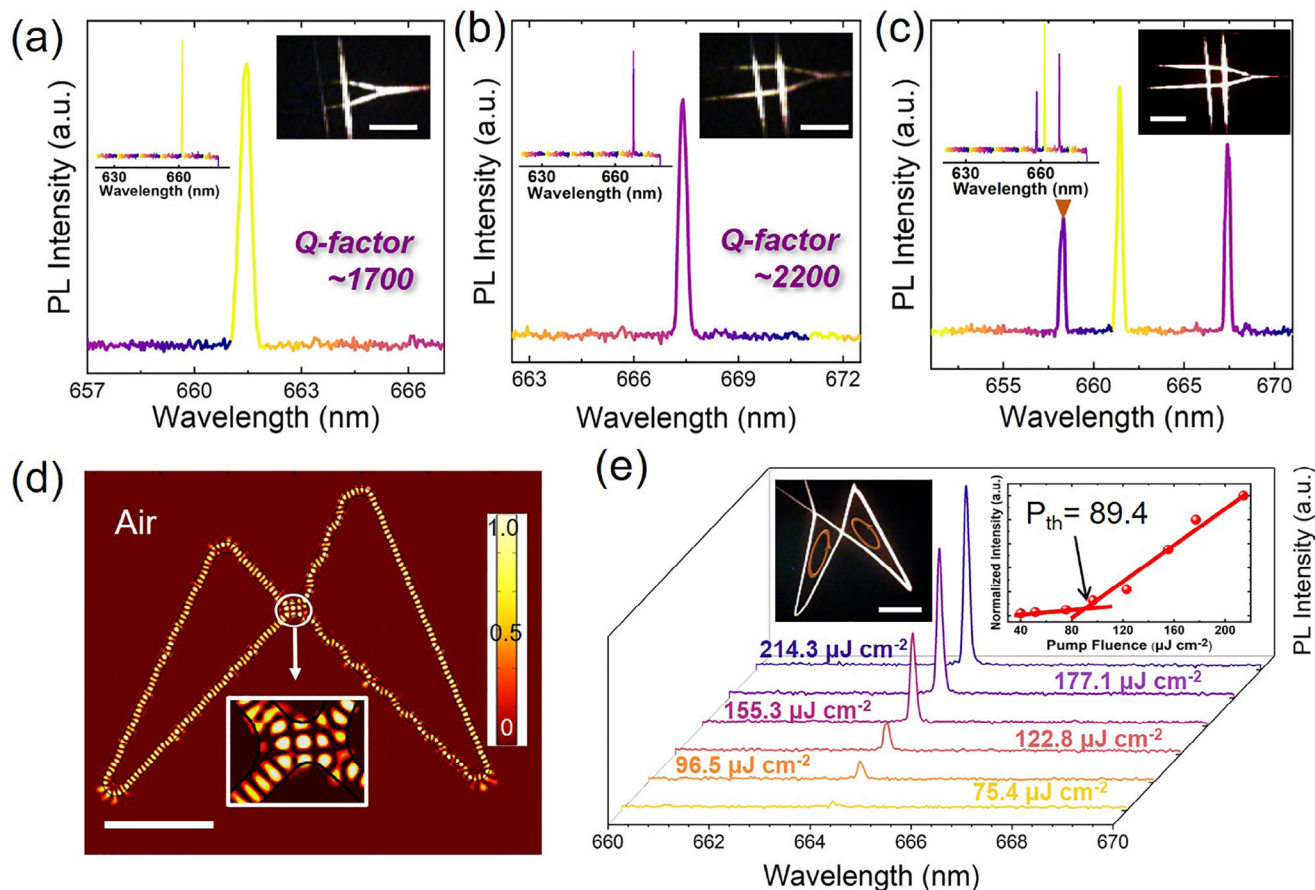


Figure 5. a) Triangular and b) quadrilateral 1-D NPLs-coated polymer microfiber lasers are used as the basic network unit for lasing emission. The Q -factor of the single frequency lasing is ≈ 1700 and ≈ 2200 respectively. c) Lasing signal from the interconnected system of two basic triangular and quadrilateral units from (a) and (b). A new peak appears at ≈ 658.3 nm (brown arrow). Scale bars: $3 \mu\text{m}$. d) Numerical simulation of electric field for a strong coupling system. The significantly enhanced electric field intensity reveals the behavior of mode coupling at the coupling point. Scale bar: $10 \mu\text{m}$. e) Lasing spectra of a strong coupling system of polygonal resonator designed, as shown in (d), under different pump intensities. The inset image shows a dark-field PL image of a strong coupling system.

(Supporting Information), the lasing thresholds of three self-coupling resonators with different shape configurations are $79.8 \mu\text{J cm}^{-2}$ (triangular), $69.4 \mu\text{J cm}^{-2}$ (quadrilateral), and $43.1 \mu\text{J cm}^{-2}$ (pentagonal). The thresholds for higher-order polygon configurations are lower than lower-order configurations. Numerical simulations confirmed the abilities of our self-coupling microresonators to support resonance modes (Figure 4b–d). Furthermore, the simulation results indicated a larger optical loss at small transmission angles compared to larger angles, providing an explanation for the lower lasing thresholds observed from higher-order resonators. We demonstrated NPLs-based polygonal self-coupling resonators with a Q -factor as high as ≈ 3500 , which is nearly one magnitude higher than contemporary 1D resonant cavities.^[21] This further affirmed the excellent optical gain characteristics of our NPLs as a gain medium.

2.4. NPLs-Based Laser Networks

Current research efforts in laser network science mainly focus on the macroscopic characterization of the overall complex system

macroscopically, often neglecting essential microscopic details. A detailed understanding of every basic unit in an optical network may be crucial for the interactions between units and the functional design of the network. To this end, we selected a triangle and quadrilateral connected to each other within a macroscopic optical topological network, as two basic units. The perimeters of these units are small enough to support only single-mode lasing (Figure 5a–c). The difference in the topological structure of the cavities manifested in variation in positions of the lasing peaks at ≈ 661.4 and ≈ 667.4 nm, respectively. This is of great significance for identifying network signals in a macroscopic system. Notably, an isolated triangular resonant cavity has a Q -factor is ≈ 1700 , whereas its quadrilateral counterpart reports a value of ≈ 2200 . Interestingly, when these two basic units are interconnected within a network, a new lasing peak at ≈ 658.3 nm is observed, in addition to the two original resonant peaks (Figure 5c). This observation provided a new understanding of signal generation from a complex topological laser network system, where the signal output is a combination of signals from individually isolated basic units and from the secondary resonant cavity formed by their mutual coupling. As a result, we can realize essential functions

such as mode coupling, wavelength tuning, signal transmission, and high-sensitivity sensing in the future, through the design and programming of basic network units.

The results from our work indicate that NPLs-based low-dimensional resonant cavities can provide sufficient optical gain and feedback necessary for laser oscillation. When the resonance conditions of two interconnected self-coupled cavities are satisfied simultaneously, one cavity can function as the spectral filter of the other. Under the interaction of two self-coupled cavities, modes that do not satisfy the common resonance conditions will be suppressed, thus enabling single-mode lasing. Based on this understanding, we designed a laser system of interconnection composed of two triangular 1D cavities to achieve single-mode lasing via resonant mode coupling. Simulation results indicate resonance mode can be simultaneously supported by two self-coupled triangular cavities (Figure 5d), with the electric field strength visibly enhanced at the coupling point to indicate the generation of mode coupling behavior. As shown in Figure 5e and Figure S17 (Supporting Information), the threshold of the single-mode lasing achieved is $89.4 \mu\text{J cm}^{-2}$, slightly higher than the isolated single 1D resonator. The numerical simulations explain the slight rise in the lasing threshold. As shown in Figure 5d, despite the enhancement of electric field strength at the coupling point, the increase of transmission angles in the interconnected triangular cavities increases scattering losses from the cavity. When the coupling structure was changed, multimode laser peaks appeared, implying that the self-coupling cavity no longer satisfied the resonance filter condition. Discrete laser peaks are identified to corresponding 1D resonant cavities, corresponding to C_1 and C_2 respectively, as shown in Figure S18 (Supporting Information). To the best of our understanding, this is the first demonstration of polygonal self-coupling resonators for modulation of single- and multimode lasing. These findings undoubtedly expand the application field of the self-coupling effect and the realization of specific lasing modes in the topological network.

3. Conclusion

In summary, we demonstrated the feasibility of colloidal NPLs-based soft matter microfiber lasers. These lasers employed CdSe/CdS@Cd_{1-x}Zn_xS core/buffer-shell@graded shell NPLs as the gain material, which exhibit an ASE threshold lower than $4.4 \mu\text{J cm}^{-2}$ and PL FWHM of ≈ 18 nm. We observed single-mode lasing (≈ 5500 Q -factor) at room temperature and conditions, which was derived from NPLs-based microfiber, as well as high stability unattainable by traditional dye fiber lasers. Furthermore, we investigated low-dimensional polygonal self-coupling lasing devices and the optical characteristics of their interconnected network. By leveraging the signal generation mechanism observed in the photonic networks, we were able to successfully design an interconnected fiber network structure based on NPLs, thereby achieving both single-mode lasing emission and laser mode modulation. Our work provides a new form of realization of on-chip integrated microlasers and mode modulation and is also of great significance to the understanding and design of basic units in future photonic network systems.

Supporting Information

Supporting Information is available from the Wiley Online Library or from the author.

Acknowledgements

R.D. and Y.T.T. contributed equally to this work. This work was supported by Nos. NRF-CRP23-2019-0007, Academic Research Fund Tier 1 (MOE-RG139/22), and AME-IRG-A20E5c0083. W.S.L. and C.X.X.L. acknowledge the support of EDB-IPP (REQ0165097). This research was supported partly by support by the Ministry of Education, Singapore, under its Academic Research Fund Tier 1 (MOE-RG62/20), Singapore Agency for Science, Technology and Research (A*STAR) MTC program, Grant No. M21J9b0085, and partly from TUBITAK 119N343, 120N076, 121C266, 121N395, and 20AG001. H.V.D. also acknowledges the support from TUBA and TUBITAK 2247-A National Leader Researchers Program (121C266).

Conflict of Interest

The authors declare no conflict of interest.

Data Availability Statement

The data that support the findings of this study are available from the corresponding author upon reasonable request.

Keywords

colloidal nanoplatelets, compositional engineering, photonic interconnected networks, self-coupling microlasers, single-mode lasing

Received: August 17, 2023

Revised: October 12, 2023

Published online:

- [1] C. Zhang, C.-L. Zou, H. Dong, Y. Yan, J. Yao, Y. S. Zhao, *Sci. Adv.* **2017**, *3*, e1700225.
- [2] B. Jiang, S. Zhu, L. Ren, L. Shi, X. Zhang, *Adv. Photonics* **2022**, *4*, 046003.
- [3] R. Duan, Z. Zhang, L. Xiao, X. Zhao, Y. T. Thung, L. Ding, Z. Liu, J. Yang, V. D. Ta, H. Sun, *Adv. Mater.* **2022**, *34*, 2108884.
- [4] S. Yang, Y. Wang, H. Sun, *Adv. Opt. Mater.* **2015**, *3*, 1136.
- [5] Y. Wang, X. Li, J. Song, L. Xiao, H. Zeng, H. Sun, *Adv. Mater.* **2015**, *27*, 7101.
- [6] N. Toropov, G. Cabello, M. P. Serrano, R. R. Gutha, M. Rafti, F. Vollmer, *Light: Sci. Appl.* **2021**, *10*, 42.
- [7] X. Jiang, A. J. Qavi, S. H. Huang, L. Yang, *Matter* **2020**, *3*, 371.
- [8] B.-B. Li, W. R. Clements, X.-C. Yu, K. Shi, Q. Gong, Y.-F. Xiao, *Proc. Natl. Acad. Sci. USA* **2014**, *111*, 14657.
- [9] S. K. Özdemir, J. Zhu, X. Yang, B. Peng, H. Yilmaz, L. He, F. Monifi, S. H. Huang, G. L. Long, L. Yang, *Proc. Natl. Acad. Sci. USA* **2014**, *111*, E3836.
- [10] R. Duan, X. Hao, Y. Li, H. Li, *Sens. Actuators, B* **2020**, *308*, 127672.
- [11] R. Parameswaran, J. L. Carvalho-De-Souza, Y. Jiang, M. J. Burke, J. F. Zimmerman, K. Koehler, A. W. Phillips, J. Yi, E. J. Adams, F. Bezanilla, B. Tian, *Nat. Nanotechnol.* **2018**, *13*, 260.
- [12] H. Zheng, Y. Zheng, N. Liu, N. Ai, Q. Wang, S. Wu, J. Zhou, D. Hu, S. Yu, S. Han, W. Xu, C. Luo, Y. Meng, Z. Jiang, Y. Chen, D. Li, F. Huang, J. Wang, J. Peng, Y. Cao, *Nat. Commun.* **2013**, *4*, 1971.

- [13] M. Hamedi, R. Forchheimer, O. Inganäs, *Nat. Mater.* **2007**, *6*, 357.
- [14] J. Feldmann, N. Youngblood, C. D. Wright, H. Bhaskaran, W. H. P. Pernice, *Nature* **2019**, *569*, 208.
- [15] R. Duan, J. Sun, Y. Zhang, H. Li, Y. Li, Z. Liu, *ACS Photonics* **2022**, *9*, 1180.
- [16] J. Feldmann, M. Stegmaier, N. Gruhler, C. Ríos, H. Bhaskaran, C. D. Wright, W. H. P. Pernice, *Nat. Commun.* **2017**, *8*, 1256.
- [17] F. Matino, L. Persano, A. Camposeo, D. Pisignano, *Adv. Opt. Mater.* **2019**, *7*, 1900192.
- [18] S. Krämmer, C. Vannahme, C. L. C. Smith, T. Grossmann, M. Jenne, S. Schierle, L. Jørgensen, I. S. Chronakis, A. Kristensen, H. Kalt, *Adv. Mater.* **2014**, *26*, 8096.
- [19] M. Gaio, D. Saxena, J. Bertolotti, D. Pisignano, A. Camposeo, R. Sapienza, *Nat. Commun.* **2019**, *10*, 226.
- [20] Y. Xiao, C. Meng, P. Wang, Y. Ye, H. Yu, S. Wang, F. Gu, L. Dai, L. Tong, *Nano Lett.* **2011**, *11*, 1122.
- [21] H. Li, J. Li, L. Qiang, Y. Zhang, S. Hao, *Nanoscale* **2013**, *5*, 6297.
- [22] L. Tong, R. R. Gattass, J. B. Ashcom, S. He, J. Lou, M. Shen, I. Maxwell, E. Mazur, *Nature* **2003**, *426*, 816.
- [23] A. Camposeo, F. Di Benedetto, R. Stabile, A. A. R. Neves, R. Cingolani, D. Pisignano, *Small* **2009**, *5*, 562.
- [24] F. Di Benedetto, A. Camposeo, S. Pagliara, E. Mele, L. Persano, R. Stabile, R. Cingolani, D. Pisignano, *Nat. Nanotechnol.* **2008**, *3*, 614.
- [25] V. D. Ta, Y. Wang, H. Sun, *Adv. Opt. Mater.* **2019**, *7*, 1900057.
- [26] X. Yang, B. Li, *ACS Macro Lett.* **2014**, *3*, 1266.
- [27] V. D. Ta, R. Chen, L. Ma, Y. J. Ying, H. D. Sun, *Laser Photonics Rev.* **2013**, *7*, 133.
- [28] R. Chen, V. D. Ta, H. Sun, *ACS Photonics* **2014**, *1*, 11.
- [29] V. D. Ta, R. Chen, H. Sun, *Sci. Rep.* **2019**, *9*, 17017.
- [30] Z. Zhang, Y. T. Thung, L. Wang, X. Chen, L. Ding, W. Fan, H. Sun, *J. Phys. Chem. Lett.* **2021**, *12*, 9086.
- [31] S. Ithurria, M. D. Tessier, B. Mahler, R. P. S. M. Lobo, B. Dubertret, A. L. Efron, *Nat. Mater.* **2011**, *10*, 936.
- [32] S. Ithurria, B. Dubertret, *J. Am. Chem. Soc.* **2008**, *130*, 16504.
- [33] M. Sharma, K. Gungor, A. Yeltik, M. Olutas, B. Guzelurk, Y. Kelestemur, T. Erdem, S. Delikanli, J. R. McBride, H. V. Demir, *Adv. Mater.* **2017**, *29*, 1700821.
- [34] Y. T. Thung, Z. Zhang, F. Yan, H. V. Demir, H. Sun, *Appl. Phys. Lett.* **2022**, *120*, 241105.
- [35] B. Liu, Y. Altintas, L. Wang, S. Shendre, M. Sharma, H. Sun, E. Mutlugun, H. V. Demir, *Adv. Mater.* **2020**, *32*, 1905824.
- [36] Y. Kelestemur, Y. Shynkarenko, M. Anni, S. Yakunin, M. L. De Giorgi, M. V. Kovalenko, *ACS Nano* **2019**, *13*, 13899.
- [37] Z. Wen, P. Liu, J. Ma, S. Jia, X. Xiao, S. Ding, H. Tang, H. Yang, C. Zhang, X. Qu, B. Xu, K. Wang, K. L. Teo, X. W. Sun, *Adv. Electron. Mater.* **2021**, *7*, 2000965.
- [38] M. Sak, N. Taghipour, S. Delikanli, S. Shendre, I. Tanriover, S. Foroutan, Y. Gao, J. Yu, Z. Yanyan, S. Yoo, C. Dang, H. V. Demir, *Adv. Funct. Mater.* **2020**, *30*, 1907417.
- [39] J. Maskoun, N. Gheshlaghi, F. Isik, S. Delikanli, O. Erdem, E. Y. Erdem, H. V. Demir, *Adv. Mater.* **2021**, *33*, 2007131.
- [40] M. D. Tessier, C. Javaux, I. Maksimovic, V. Lorette, B. Dubertret, *ACS Nano* **2012**, *6*, 6751.
- [41] M. Olutas, B. Guzelurk, Y. Kelestemur, A. Yeltik, S. Delikanli, H. V. Demir, *ACS Nano* **2015**, *9*, 5041.
- [42] C. She, I. Fedin, D. S. Dolzhenkov, A. Demortière, R. D. Schaller, M. Pelton, D. V. Talapin, *Nano Lett.* **2014**, *14*, 2772.
- [43] A. Naeem, F. Masia, S. Christodoulou, I. Moreels, P. Borri, W. Langbein, *Phys. Rev. B* **2015**, *91*, 121302.
- [44] S. Delikanli, O. Erdem, F. Isik, H. Dehghanpour Baruj, F. Shabani, H. B. Yagci, E. G. Durmusoglu, H. V. Demir, *J. Phys. Chem. Lett.* **2021**, *12*, 2177.
- [45] L. T. Kuneman, M. D. Tessier, H. Heuclin, B. Dubertret, Y. V. Aulin, F. C. Grozema, J. M. Schins, L. D. A. Siebbeles, *J. Phys. Chem. Lett.* **2013**, *4*, 3574.
- [46] J. Yu, C. Dang, *Cell Rep Phys Sci* **2021**, *2*, 100308.
- [47] C. E. Rowland, I. Fedin, H. Zhang, S. K. Gray, A. O. Govorov, D. V. Talapin, R. D. Schaller, *Nat. Mater.* **2015**, *14*, 484.
- [48] Y. T. Thung, R. Duan, E. G. Durmusoglu, Y. He, L. Xiao, C. X. X. Lee, W. S. Lew, L. Zhang, H. V. Demir, H. Sun, *Laser Photonics Rev.* **2023**, *17*, 202200849.
- [49] J. Q. Grim, S. Christodoulou, F. Di Stasio, R. Krahn, R. Cingolani, L. Manna, I. Moreels, *Nat. Nanotechnol.* **2014**, *9*, 891.
- [50] J. Yu, M. Sharma, M. Li, S. Delikanli, A. Sharma, M. Taimoor, Y. Altintas, J. R. McBride, T. Kusserow, T. C. Sum, H. V. Demir, C. Dang, *Laser Photonics Rev.* **2021**, *15*, 2100034.
- [51] C. She, I. Fedin, D. S. Dolzhenkov, P. D. Dahlberg, G. S. Engel, R. D. Schaller, D. V. Talapin, *ACS Nano* **2015**, *9*, 9475.
- [52] Y. Gao, M. Li, S. Delikanli, H. Zheng, B. Liu, C. Dang, T. C. Sum, H. V. Demir, *Nanoscale* **2018**, *10*, 9466.
- [53] Z. Yang, M. Pelton, I. Fedin, D. V. Talapin, E. Waks, *Nat. Commun.* **2017**, *8*, 143.
- [54] R. Momper, H. Zhang, S. Chen, H. Halim, E. Johannes, S. Yordanov, D. Braga, B. Blülle, D. Doblás, T. Kraus, M. Bonn, H. I. Wang, A. Riedinger, *Nano Lett.* **2020**, *20*, 4102.